DREMUS: A Data-Restricted Multi-Physics Simulation Model for Lithium-Ion Battery Storage

Martin Rogall, Anup Barai, Maria Brucoli, Patrick Luk, Rohit Bhagat, and David Greenwood

DOI 10.1016/j.est.2020.102051
ISSN 2352-152X

Publisher: Elsevier

Journal of Energy Storage 32 (2020) 102051

Contents lists available at ScienceDirect

Journal of Energy Storage

journal homepage: www.elsevier.com/locate/est

DREMUS: A Data-Restricted Multi-Physics Simulation Model for Lithium-Ion Battery Storage

Martin Rogall [a,*], Anup Barai [a], Maria Brucoli [b], Patrick Luk [c], Rohit Bhagat [d], David Greenwood [a]

[a] WMG, The University of Warwick, Coventry CV4 7AL, UK
[b] EDF Energy, Interchange, 81- 85 Station Rd, Croydon CR0 2AJ, UK
[c] Cranfield University, College Rd, Cranfield, Wharley End, Bedford MK43 0AL
[d] Coventry University, Priory St, Coventry CV1 5FB

A B S T R A C T

This paper presents a modelling approach to support the techno-economic analysis of Li-Ion battery energy storage systems (BESS) for third party organisations considering the purchase or use of BESS but lacking the detailed knowledge of battery operation and degradation. It takes into account the severe data-limitations and provides the best possible approximation for its long-term electrical, thermal and ageing performance. This is achieved by constructing flexible and scalable ageing models from experimental data based on manufacturer's datasheets, warranties and manuals as key inputs. The precision of the individual models has been determined using experimental data and has been found with <8 % normalised root-mean-square deviation (NRMSD) in all cases to be sufficiently accurate. Through linearization methods, this model is able to compare the long-term performance of BESS and quantify the degradative impact of specific charge/discharge mission profiles, which improves the tangibility of BESS as value generating asset.

Introduction

Battery energy storage systems (BESS) are an essential part of a sustainable energy system, due its capability to defer generation and consumption in time and thus support balancing demand and supply, both locally and on grid-scale. The fast reaction time of BESS is especially useful to counter the volatility of solar and wind power and consumers in general. Currently, the most established and reliable market-available technology for BESS is Lithium-Ion, which provides high efficiency, high energy density and long cycle life [1].

For a widespread deployment of BESS with sustainable energy systems, they must be commercially viable. As assets with high upfront costs, BESS face several challenges considering their viability; they are complex systems with uncertain degradation behaviour due to the manifold mechanisms causing it [2] and limitations of non-destructive diagnostic techniques [3]. A significant challenge for end-users of BESS is the limitation in data provided on the BESS – especially relative to a specific target usage profile. This restricts direct comparison of different BESS from different suppliers. Understanding battery value degradation given its utilisation and how service-life of the BESS can be extended will determine whether investment in a specific BESS provides a justified return.

A common method to support viability is to model BESS. Many authors have developed such models [4–15]. Nevertheless, there are several issues some or all of these models and approaches share:

- Inflexibility: The approach taken is outlined for limited Li-Ion chemistries [5,8–15] or use cases [4,5,7,8,10–12,14,15]. For example, the authors of [10] specifically utilised an ageing model for one type of NMC cell to estimate the feasibility of energy arbitrage in four markets. Likewise the model in [14] optimised the operation of LFP batteries for the provision of frequency response in the UK. Both of these approaches cannot be translated into other use cases or applied for different battery chemistries.
- One-dimensionality: Few models consider a full multi-physics approach. Further they are often based on phenomenological rather than physicochemical behaviour [4,6,8,10,12,14,15]. The model used in [10], for instance, utilises a Joule-based electrical model and a purely empirical ageing model. This approach is a significant simplification that is not robust towards any changes in the BESS or utilisation and does not consider proven degradation impact factors such as the C-Rate and temperature damaging its accuracy.
- Data Availability: Many studies rely on a significant amount of data on the battery and may only work with historical data on the actual battery [5,8,9,13]. For example the model in [8] utilises an ageing model constructed from experimental data on that battery. That data can only be obtained by investing in the battery and testing beforehand.

* Corresponding author.

https://doi.org/10.1016/j.est.2020.102051
Received 8 May 2020; Received in revised form 11 September 2020; Accepted 2 November 2020
Available online 21 November 2020

While the models developed for a specific chemistry, phenomenological behaviour or with a particular battery specific dataset, can yield in good performance estimation, they are also limited in their capability to estimate the behaviour of a different battery. To do so, often they will require either specific training dataset from the new battery of interest, or values of specific parameters, which can only be achieved through in-situ analysis. This may not be a problem for OEMs and research organisation; however, this is especially of concern to third-party purchasers (not associated or experienced with battery manufacturing, market or modelling) of BESS, such as companies interested in optimisation of their renewable energy plants, provision of flexibility services (e.g. demand side response) or demand peak shaving. These investors need to assess BESS from different manufacturers, often with limited information. The BESS need to be assessed for all the application specific use cases, calculating asset depreciation due to degradation and allowing an informed decision for the overall investment viability.

Currently, in literature, there is limited research reporting generic battery models, which can make a performance and degradation estimation of any available battery with limited information. The likely reason might be that estimation by such model will have higher level of embedded errors compared to battery specific models. This paper describes such a modelling approach, designed to counter these issues, and based on the limited data typically available,. The model is constructed from generic chemistry related cell behaviour, experimental data providing battery sensitivity to input parameters and reference data, and the common, commercially available information on the BESS in the shape of datasheets, warranties and manuals. The complete model is designed to be capable of forecasting the BESS's long-term performance and specifically the expected degradation rate under any given usages condition.

Model Development

The modelling approach in this paper is dubbed Data-REstricted MUlti-physics Simulation (DREMUS). The constraints on the model are only due to data limitations during application, meaning that the user will not require further information or experimental data. Data generally provided in datasheets and warranties on the BESS and required for the applicability of this model include energy capacity, nominal voltage, efficiency, conditions of the end-of-life and cathode material.

DREMUS has three primary purposes: comparison of long-term BESS performance (including degradation), comparison of service provision impacts and long-term feasibility analysis. To achieve this, the model must provide a way to objectively compare the ageing rate of different BESS and during different operations of said BESS. That ageing rate must be comparable between BESS.

Model Structure

For a stationary enclosed storage system, two main factors associated with the proposed application need to be considered: electrical utilisation and environmental temperature. Other factors such as humidity, pressure and possible physical hazards are generally considered constant or negligible. To capture these impacts, an electrical and thermal model are required to evaluate their dynamics. Further, an ageing model needs to capture and update the impact on the BESS. It is important to note that all three models are strongly interdependent and need to be constantly updated.

An overview of the model structure of DREMUS is shown in Figure 1. The core model is based on three interconnected sub-models (electrical, thermal and ageing), which run in parallel. The electrical model provides heating data to the thermal model and receives the cell temperature to adjust the electrical behaviour. Thermal and electrical data influence the cell ageing, which consequently affects the electrical behaviour as well.

In the first step, the battery documentation is used to scale the

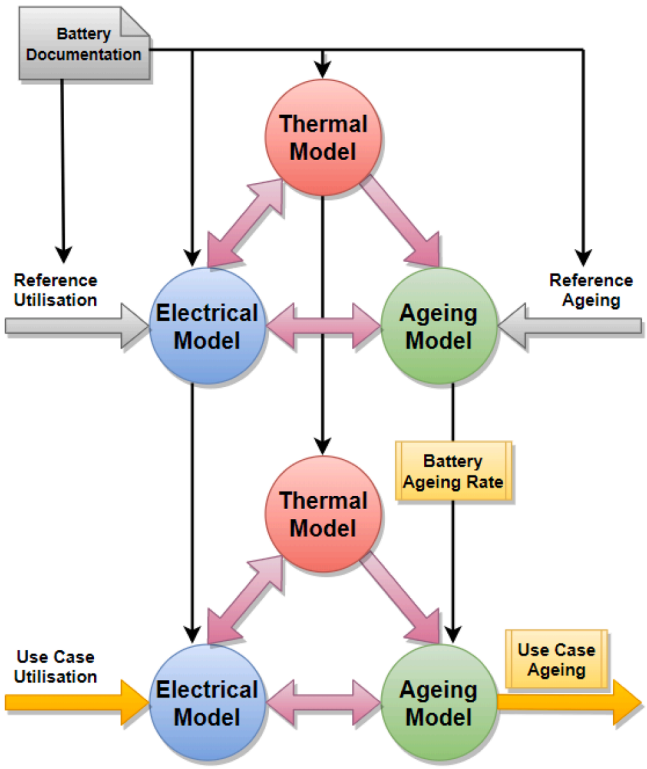

Figure 1. DREMUS model structure.

electrical and thermal models to the given BESS. Using a given datapoint for degradation (cycling/environmental conditions under which terminal end-of-life capacity is reached), the ageing model is then scaled as well by determining the battery specific ageing rate.

The input for the completed model is the charge/discharge mission profile of the use case, describing the power demand of the BESS for a pre-determined method of value generation (e.g. frequency response, STOR…). If known, changes in environmental temperature can be included as well. The output is the expected degradation of the BESS as a function of time/usages. A visual representation of the application of DREMUS to evaluate expected ageing rate under proposed use cases is given in Figure 2, with the state of health (SoH) as a measure of relative remaining capacity.

Resources

The pre-requisite of this model is the standard information given before acquisition on the BESS. This information is commonly provided in datasheets, manuals and warranty conditions for both battery and

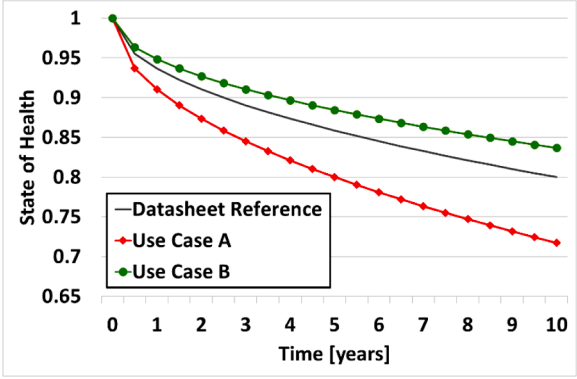

Figure 2. Exemplary application of DREMUS for health estimation.

converter. This information allows to scale the model for electrical and ageing behaviour, but does not provide sufficient details for the entirety of the required model. The remainder of the model must therefore be pre-determined using other information sources, such as literature and experimental data.

Literature provides general references to specific chemistries and the behaviour of Li-Ion batteries, such as curves for open-circuit-voltage, entropy and equivalent circuit models. Although these values and models vary between manufacturers and individual cells, the general behaviour and limits are dominated by their chemistry [16,17].

Experimental data allows for quantification of sensitivities towards impacting factors on the ageing behaviour, as well as numerical references for typical electrical and thermal behaviour. If possible, those references should be scaled to available data on the given BESS. An overview on the input parameters and curves is given in Table 1.

The three core models of DREMUS for BESS are created using this method, prioritising available data on the BESS and supplementing it with information gathered from literature and experimental data.

Experimental Data

Experimental data is necessary for the electrical, thermal and ageing model, to provide scalable behaviour and an architectural reference. Two different cell types are referenced, the data of which are outlined in Table 2.

The first dataset contains pre-collected calendric and cyclic ageing data on 18650 cells of Type A. The calendric tests were performed at environmental temperatures between 10 and 60°C. The cyclic tests were performed at room temperature with 0.3 C charge and between 0.4 and 1.2 C discharge.

The tests of type B were performed by the author under accelerated conditions (50°C environmental temperature in a Vötsch VC3 4060 climatic test chamber) and under various mission profiles, namely provision of arbitrage trading and Enhanced Frequency Response, daily full cycling and micro-cycling. The use of 50°C was chosen with the intent to provide acceleration of ageing mechanisms without triggering additional mechanisms which will not be present at room temperature [18]. The cycling was performed with a Digatron BTS-600 battery cycler. Temperature data has been collected through the cycler thermocouple itself on the module surface and through Picolog 1216-coupled thermistors inside the module.

Electrical Model

To emulate the electrical behaviour of a BESS, three main subsystems must be considered: converter, battery and cell. The incoming signal of charge and discharge power must be translated into cell current. A charge (of the battery) will be denoted as positive and a discharge as negative power/current.

Table 2
Cell data.

	TYPE A	TYPE B
CELL CAPACITY	3 Ah	33 Ah
DC RESISTANCE	0.0413	0.0030
CHEMISTRY	NMC	NMC-LMO
ARCHITECTURE	Cylindrical	Pouch
CONFIGURATION	1s1p	2p2s
BRACING	No	Yes
CELL COUNT	51	20
CALENDRIC TEST	10-60°C	50°C
	20-90 % SoC	50 % SoC
CYCLIC TEST	25°C	50°C
	0.3/0.4 C – 0.3/1.2 C	Mission Profiles
	30-80 % DoD	

Converter

The converter, interfacing the batteries with the AC (or in some cases DC) grid can be considered the main control unit of the BESS. A significant amount of data on converters can be drawn from datasheets and manuals, including voltage ratings, power limitations and efficiency.

The power drawn from the battery depends mainly upon the efficiency of the converter. For roundtrip efficiencies, the unidirectional efficiency can be calculated as its square-root:

$$\eta_{con,u} = \sqrt{\eta_{con,r}} \tag{1}$$

$$P_{bat} = \begin{cases} P_{con} * \eta_{con,u} \; for \; P_{con} > 0 \\ \dfrac{P_{con}}{\eta_{con,u}} for \; P_{con} < 0 \end{cases} \tag{2}$$

An important factor for this efficiency is its dependency upon the power drawn (as percentage of its nominal power). The authors of [19] have shown the general efficiency behaviour of transformer based and DC-DC based converters. They show that especially low power utilisation (< 20% transformer, <5 % DC-DC) can significantly reduce efficiency.

The provided efficiency-power curves can be scaled using the efficiency in the datasheet, specifically by using the maximum efficiency as follows:

$$P_{con,\%} = \frac{P_{con}}{P_{con,n}} \tag{3}$$

$$\eta_{con,u}(P_{con}) = \eta_{con,u}^{max}\left(\frac{16.470}{P_{con,\%} + 16.162} - \frac{2.657 * 10^{-4}}{{P_{con,\%}}^2}\right) \tag{4}$$

Table 1
Input parameters and curves sorted by sources.

Datasheet Inputs		Literature Inputs		Experimental Inputs	
Converter					
$P_{con,n}$	Nominal	$\eta_{con,u}(P_{con})$	Efficiency Curve		
$\eta_{con,r}^{max}$	Maximum Roundtrip Efficiency				
Battery					
	Cathode Chemistry	E_a	Resistance Activation Energy	$R_{DC}(SoH_{abs})$	Resistance-Capacity Curve
Q_0	Capacity	$U_{oc,ref}(SoC)$	Open-circuit voltage curves	$\frac{R_1}{R_0}$	ECM resistance proportion
$U_{oc,n}$	Nominal Voltage	$\frac{\partial U_{oc}}{\partial T}(SoC)$	Entropy curves	τ	ECM Time Constant
I_n	Nominal Current	$U_n(SoC)$	Anode potential curve	κ_x	Thermal conductivities
$\eta_{bat,r}$	Roundtrip Efficiency			C_{cell}, C_{mod}	Thermal capacitances
$P_{ref}(t)$, $I_{ref}(t)$	Reference Utilisation			k_x	Ageing Fitting Parameters
SoH_{eol}	End-of-life Capacity				
T_n	Nominal Temperature				

$$\eta_{con,u}(P_{con}) = \eta_{con,u}^{max}\left(\frac{1.283}{P_{con,\%}+0.076} - 0.230 * P_{con,\%}\right) \quad (5)$$

$P_{c,\%}$ is the relative power on the converter, which is the power on the converter P_c divided by its nominal power $P_{c,n}$. Equations (4) and (5) refer to DC-DC converters and transformer converters, respectively. If the precise efficiency curves are given for the converter, they should be used instead.

Battery

In the next step the parameters of the battery must be determined. Initially it is modelled as a single element. Capacity and voltage are commonly given, the resistance, however, is only given as a value of efficiency. An estimate for DC resistance can be determined from the battery roundtrip efficiency $\eta_{bat,r}$, nominal current I_n and nominal voltage $U_{oc,n}$. This is achieved by comparing the input and output energy of a single-resistance model:

$$\eta_{bat,r} = \frac{E_{out}}{E_{in}} \quad (6)$$

$$E_{out} = E_{in} - |I_n|^2 R_{bat} t_{ch} - |I_n|^2 R_{bat} t_{dch} \quad (7)$$

$$E_{in} = |I_n| U_{bat,n} t_{ch} + |I_n|^2 R_{bat} t_{ch} \quad (8)$$

$$t_{ch} = t_{dch} \quad (9)$$

$$\eta_{bat,r} = 1 - \frac{2|I_n| R_{bat}}{U_{oc,n} + |I_n| R_{bat}} \quad (10)$$

$$\frac{(1-\eta_{bat,r}) U_{bat,n}}{(1+\eta_{bat,r})|I_n|} = R_{bat} \quad (11)$$

This approach assumes symmetrical resistance. It is also based on the nominal/averaged conditions of the battery and does not account for potential coulombic or cable losses. However, without any additional data, this is the closest approximation to the DC resistance available.

The datasheet of the cell type A does not provide an efficiency value, but an indication of the initial DC resistance of 0.0413 Ohms. Using equation (10) for a nominal current of 0.5 C, the approximate efficiency of the cell results in 96.7%, which is typical for a Li-Ion battery efficiency. The efficiency for type B is 97.4 %. While an exact value of the cell resistance cannot be determined, the equation will provide a good approximation of the DC resistance, being as accurate as the information given in the datasheet.

Since a battery consists of multiple cells those parameters along with the input power need to be distributed across the individual cells in the battery. For that, the structure of the battery must be known, which commonly follows a combination of serial and parallel connections [20]. For simplicity, a parallel connection of multiple strings can be assumed. This will support the model construction.

The number of strings in parallel n may be given for the BESS or the number of BESS installed, since the battery voltage must stay constant to be compatible with the inverter. The number of cells in series m can be determined using the battery nominal voltage and cell chemistry nominal voltage:

$$m = \frac{U_{bat,n}}{U_{cell,n}} \quad (12)$$

For added precision, the module of type B can be chosen as reference, wherein each string consists of 2p2s modules in series. The number of cells and subsequent calculations have to be amended accordingly.

To determine the resistance of individual cells the rules of parallel and series connection can be applied under the assumption that all cells have equal characteristics in their initial state:

$$R_{bat} = \frac{1}{\sum_{i=1}^{n} \frac{1}{R_{str,i}}} \quad (13)$$

$$R_{str} = n * R_{bat} \quad (14)$$

$$R_{str} = \sum_{i=1}^{m} R_{cell,i} \quad (15)$$

$$R_{cell} = \frac{R_{str}}{m} \quad (16)$$

It is recommended to model all cells and their individual behaviour separately and introduce parameter variability where data is available. If that approach is chosen, an appropriate BMS must be simulated as well.

A simpler approach is to focus on a single cell and divide the total power drawn by the total number of cells. The advantage of this approach is the reduction in data requirements and the lower computational requirements. Since data on the variability and BMS is currently not available, the rest of this paper focusses on this latter approach.

Cell

The value for battery resistance is commonly affected by temperature as Arrhenius dependency [21,22]:

$$R_{DC} = R_{DC,0} * e^{\frac{-E_a}{R_g} * \left(\frac{1}{T_n} - \frac{1}{T_{cell}}\right)} \quad (17)$$

The activation energy E_a varies in literature between 14 and 29 kJ/mol [21–25] with no apparent connection to chemistry or architecture. Although no data has been provided for cell type A, the data collected on the Type B cells showed values on the lower end of this spectrum and steady decline far below this spectrum over time. Therefore 14 kJ/mol was assumed as average value over time.

The final dependency of the DC resistance is upon the state-of-health (SoH; relative remaining capacity as defined in section 3.4) of the cell. A generally linear dependency upon the 60-80 % SoH (as measure of relative retaining capacity) has been identified in literature [26–28] and has been confirmed through the experimental data obtained from the cells A and B as shown in Figure 3.

It should be noted that the data is subject to scattering, most likely due to inaccuracies, mild cell state differences and changing contact resistances. Overall, the linear dependency best represents the development for both individual cell types.

The increase in resistance is slightly different between the two types. To represent the average resistance increase of both cells, the red line of Figure 3 can be described by the following equation:

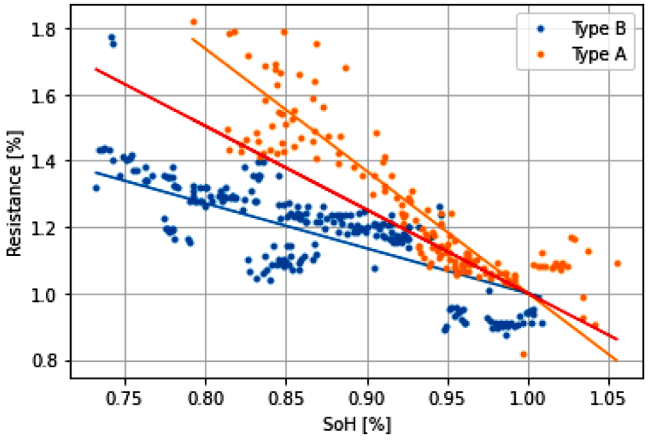

Figure 3. DC Resistance in dependency of the SoH.

$$R_{DC}(SoH_{abs}) = R_{DC,0}(-2.525 * (SoH_{abs} - 1) + 1) \quad (18)$$

Thus, through linear combination of equation (17) and (18) the behaviour of the cell DC resistance is expressed as:

$$R_{DC} = R_{DC,0}(-2.525 * (SoH_{abs} - 1) + 1) * e^{\frac{-14\frac{kJ}{mol}}{R_g}\left(\frac{1}{T_{ref}} - \frac{1}{T_{cell}}\right)} \quad (19)$$

For an approximation of the transient behaviour of battery cells, a reference equivalent circuit model (ECM) is required. Commonly, transient ECMs contain one to two RC elements and a series resistance [29–31]. The charge/discharge response of the tested cells were found to be modelled with one RC-element with sufficient accuracy (0.49% NRMSD for type B). Data on the single-RC circuit has been provided. Added complexity to the model would also make a good approximation more difficult. The full ECM is displayed in Figure 4.

The individual elements of the ECM can be determined using the DC resistance as scaling value and estimates for relative values, specifically $\frac{R_1}{R_0}$ and the R_1C_1 time constant τ:

$$R_0 = \frac{R_{DC}}{\frac{R_1}{R_0} + 1} \quad (20)$$

$$R_1 = R_{DC} - R_0 \quad (21)$$

$$C_1 = \frac{\tau}{R_1} \quad (22)$$

The graphs in Figure 5 show the development of $\frac{R_1}{R_0}$ and τ over different SoH, as provided by the database for type A and fitted to a C/2 charging pulse at 50 % SoC for type B. It is apparent that there is no definitive connection between those parameters and the ageing of the cell, especially when comparing two different cell types. However, they generally stay within the same range, even though the architecture and size of the two cells were very different. Therefore the average was used as reference.

The average values for $\frac{R_1}{R_0}$ and τ are 0.52 and 41.91 s, respectively. Pulse characterisation from literature [32,33] displays values in a similar range when interpreted by a R-RC circuit, further verifying it as a sufficient approximation.

It should be noted that these values may vary between cell manufacturers, sizes and design intents (energy/power cells) and merely serve as a reference to include transient behaviour reflective of real cells.

Additional to the passive elements, the ECM contains a voltage source representing the open-circuit-voltage (OCV) of the cell in dependence of the state-of-charge (SoC; percentage of contemporary capacity). This dependency is mainly set by the chemistry and several authors provide lookup tables and equations for each [16,26,34,35].

The temperature dependent modification of the OCV is tied to the cell entropy [36], for which several authors provide lookup tables as well [17,23,36–38]. Thus, the total OCV for any given SoC is:

$$U_{oc} = U_{oc,ref}(SoC) + \frac{\partial U_{oc}}{\partial T}(SoC) * (T_{cell} - T_{ref}) \quad (23)$$

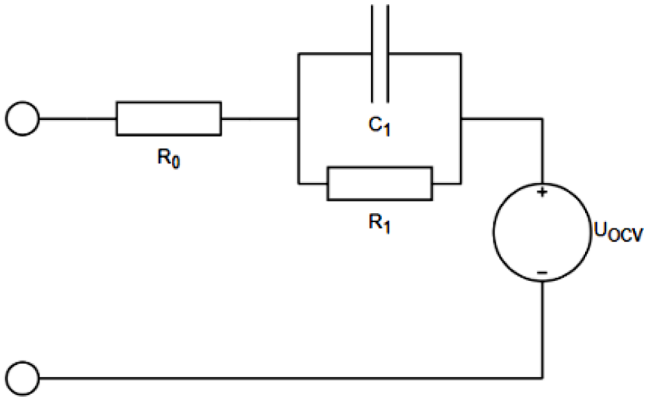

Figure 4. Electrical ECM.

Thermal Model

The thermal model can again be described by an equivalent circuit model. The structure of the BESS is generally unknown, making the construction of a detailed model very difficult. Therefore, the tested cells and modules serve as reference.

The module of the cells of type B provides a reference for thermally constrained, passively cooled cells. Four cells are stacked upon each other in an open aluminium case. Between the case and the cells is a protective polymer, reducing thermal conductivity κ_{mod}. The temperature was measured on the surface of the module case and in-between the cells. The equivalent circuit for this module is given in Figure 6.

Initial tests have shown that the cell-to-cell thermal resistance is, compared to the module and convection resistance, small enough to be neglected. Therefore, the cells have been combined into one thermal node and q_{cells} represents the combined heat generation of all four cells. The polymer layer is assumed to have a thermal capacitance C_{mod} as well as a thermal resistance.

Using passive cooling measurements of the module, the parameters of this model have been fitted as shown in Table 3. The NRMSD of this model approximating the cooling behaviour is 1.07 %.

Some BESS may provide active cell temperature control, which may reduce ageing processes. In that case, it would be recommended to use a single cell ECM instead as displayed in Figure 7, since this model omits cell to cell interactions. This ECM is in reference to the cylindrical cells of Type A.

T_{amb} can be substituted by the coolant temperature if known. The parameters for this model have been provided as given in Table 4.

The heat generation of Li-Ion cells is primarily bound to Ohmic (caused by electrical resistance, q_{ohm}), reactive (caused by electrode overpotential, q_{reac}) and entropic (caused by reversible chemical reaction, q_{ent}) heat [39,40]:

$$q_{cell} = q_{ohm} + q_{reac} + q_{ent} \quad (24)$$

The purely Ohmic resistance and the resistance caused by the electrode overpotential are electrically indistinguishable and can therefore both be captured by heat development of the electrical ECM:

$$q_{res} = q_{ohm} + q_{reac} = {I_{R0}}^2 R_0 + {I_{R1}}^2 R_1 \quad (25)$$

The entropic heat is caused by the chemical reactions within the cell, which depend on the cell chemistry. Lookup tables by the authors of [17,23,36–38] provide data for $\frac{dU_{OC}}{dT}/\Delta S$ for different SoC. The entropic heat is then calculated as follows:

$$q_{ent} = I * T * \frac{\Delta S}{nF} = I * T * \frac{dU_{OC}}{dT} \quad (26)$$

It is important to note that in contrast to Ohmic and overpotential heat, the entropic heat is dependent on the direction of the current and can therefore cool the cell as well.

The thermal models above refer to the specific cells of type A and B. Therefore, the heat generation needs to be scaled to the respective cell properties. Since entropic and ohmic heating are dependent upon different factors, they must be scaled differently. Entropic heating is dependent upon the entropy change, which is connected to the SoC and therefore already relative, and the charge current, which can be directly scaled by the cell capacity:

$$q_{ent,ref} = q_{ent} * \frac{Q_{ref}}{Q_0} \quad (27)$$

Q_{ref} is the cell capacity of type A or B, Q_0 is the nominal cell capacity of the chosen battery, q_{ent} is the entropic heat generated and $q_{ent,ref}$ is the

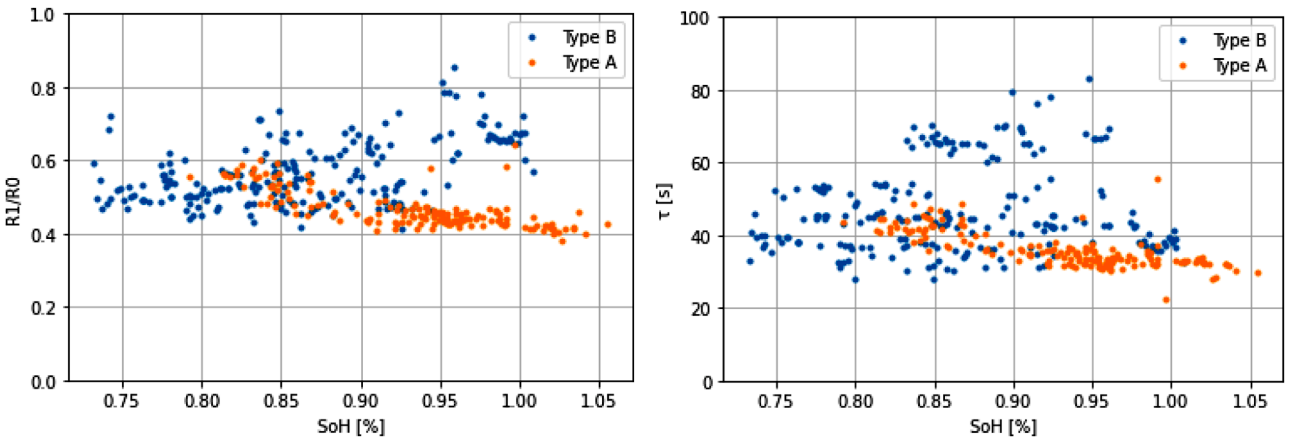

Figure 5. $\frac{R_1}{R_0}$ and τ over different SoH.

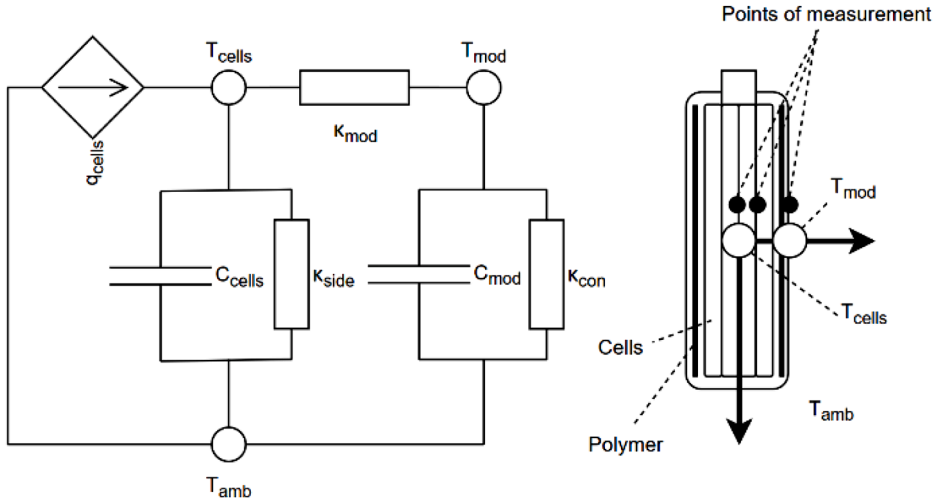

Figure 6. Type B module bulk thermal ECM.

Table 3
Parameters of the module thermal ECM based on Type B.

PARAMETER	VALUE	UNIT
C_{cell}	3.512e+03	J/K
C_{mod}	2653e+02	J/K
κ_{side}	8.878e-01	W/K
κ_{mod}	4.891e-03	W/K
κ_{conv}	1.313e-01	W/K

equivalent heat generation in the reference cell model.

Ohmic heating is dependent upon to the cell resistance and the square current, and should therefore be scaled by the cell resistance and the square of the cell capacity:

$$q_{res,ref} = q_{res} * \frac{R_{ref}}{R_0}\left(\frac{Q_{ref}}{Q_0}\right)^2 \tag{28}$$

R_{ref} is the DC cell resistance of type A or B, R_0 is the nominal DC cell resistance of the chosen battery, q_{res} is the resistive heat generated and $q_{res,ref}$ is the equivalent heat generation in the reference cell.

It should be noted, that to apply the module model of type B, the overall heat generation needs to be multiplied by the cell count in the model, which is four.

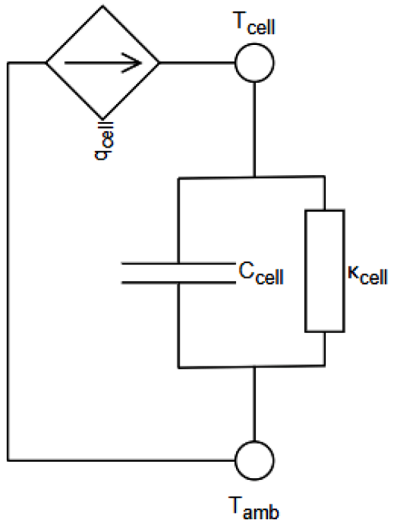

Figure 7. Type A cell bulk thermal model.

Ageing Model

Model Development

The absolute degradation of the cell will be quantified by its capacity

Table 4
Parameters of the cell thermal ECM based on Type A.

Parameter	Value	Unit
C_{cell}	83.3704	W/K
κ_{cell}	0.1605	W/K

fade as follows:

$$SoH_{abs,t} = \frac{Q_t}{Q_0} \tag{29}$$

The authors of c characterise SEI formation as the primary ageing mechanisms for carbon-anode cells. Several authors have created electrochemical ageing models on that premise [41–43], which closely resemble an Arrhenius dependency. The base for this ageing model is the equation for the side reaction current as given in [44]. The parameters of this model are given in Table 5.

$$Deg_1 = \int i_{os} \exp\left(-\frac{\alpha_c F}{RT}\left(U_n - U_{ref,s} - i_t\left(R_{SEI} - \frac{M_{SEI}}{\kappa_P F \rho_{SEI}} * Deg_0\right)\right)\right) dt \tag{30}$$

There are several issues of practicality and accuracy in in this model which need to be modified to be applicable in DREMUS. The first issue is that the time dependency differs from most observations of the capacity loss of Li-Ion cells, which generally resemble a square-root dependency ([26,45–49]) until the EOL capacity is reached. This model indicates a steadily increasing capacity fade.

To adjust for this, it is firstly assumed that the SEI/film resistance is comparatively constant before reaching the EOL. This linearizes the function. Further, this linearized degradation can be translated to absolute degradation using a square-root dependency:

$$SoH_{lin,1} = SoH_{lin,0} - Deg_{lin,1} \tag{31}$$

$$SoH_{abs} = 1 - \left(1 - SoH_{abs,eol}\right) * \sqrt{1 - SoH_{lin}} \tag{32}$$

SoH_{lin} is the linear state-of-health, Deg_{lin} is the linear degradation and $SoH_{abs,eol}$ is the terminal SoH (denoting the onset of non-linear ageing processes aka knee-point, at which this equation is no longer applicable). To provide a general reference, $SoH_{abs,eol}$ has been set to 80 %, since it is generally referred to as the EOL criteria [50].

Further, i_t is a relative parameter depending upon the active surface area of the cell, which is unknown. Considering that this area is proportional to the cell capacity (for identical electrode thickness), it can be replaced by the C-rate.

$$c = \frac{I}{Q_0} \tag{33}$$

Under these modifications, the dependency upon temperature, anode potential and current is preserved. However, the local constants cannot be applied in their original way and have to be replaced by fitting parameters:

$$Deg_{lin} = \int k_1 \exp\left(-\frac{k_2}{T}\left(U_n - k_3 - k_4 c\right)\right) dt \tag{34}$$

U_n is dependent upon the SoC. The carbon anode potential curve variation with the anode SoC is displayed in Figure 8. Commercial cells likely only partially utilise the anode to avoid ageing processes triggered by over/under-potential (e.g. Lithium plating, current-collector corrosion [51]). This must be accounted for using additional fitting parameters.

$$SoC_n = SoC_{cell} * k_m + k_n \tag{35}$$

All parameters have been fitted to the ageing data of type A. The parameters, along with the applied boundary conditions are listed in Table 6.

These parameters describe the dependency upon the different impact factors, as well as the ageing rate of the cell type A. The overall NRMSD of this ageing model in forecasting the next ageing state is approximately 7.2 %. This can partially be explained through unexpected capacity recoveries and other outliers. Overall the model should be able to represent the averaged behaviour of many cells.

It should be noted that the ageing data of both Type A and B above 40°C displayed disproportionate capacity loss, indicating additional, unwanted ageing processes. This is in agreement with the findings in [53]. Since this behaviour cannot be represented using the ageing equation, that data has been excluded from the fit. Since operation beyond 40°C is generally not to be expected in regulated stationary storage systems and very unfavourable, it will be considered a soft constraint in the model, meaning that the model is generally not applicable in higher environmental temperatures but should still be allowed to handle short periods above 40°C incurred through cell heating.

Datasheet Validation

The datasheet provided with the cells of type A contains an estimated ageing curve. This curve is displayed in Figure 9. It needs to be noted that the initial capacity is higher than the nominal capacity. This has been taken into account using the model estimation displayed.

The datasheet slightly overestimates the ageing in comparison to the

Table 5
Constants and variables of the SEI degradation equation [44].

	Value	Unit	Meaning
Local Constants	i_{0s}	$\frac{A}{m^2}$	Side reaction exchange current density
	α_c		Anode charge transfer coefficient
	$U_{ref,s}$	V	Side reaction equilibrium potential
	R_{SEI}	$\frac{\Omega}{m^2}$	SEI resistance
	M_{SEI}	$\frac{kg}{Mol}$	SEI molecular weight
	κ_P	$\frac{S}{m}$	Anode activation energy
	ρ_{SEI}	$\frac{kg}{m^3}$	SEI density
Global Constants	F	$\frac{As}{mol}$	Faraday constant
	R	$\frac{J}{Kmol}$	Boltzmann constant
Independent Variables	T	K	Temperature
	U_n	V	Anode potential
	i_t	$\frac{A}{m^2}$	Current
	t	h	Time

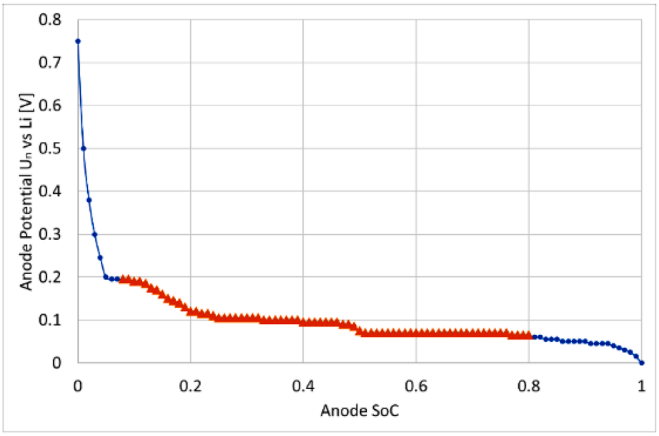

Figure 8. Anode Potential Curve [52].

Table 6
Ageing Model Fitting Parameters based on type A.

Parameter	Bounds		Value	Unit
k_1	0	$+\infty$	1.441e-08	s^{-1}
k_2	0	$+\infty$	3.352e+03	KV^{-1}
k_3	0	$+\infty$	1.230e-02	V
k_4	0	$+\infty$	8.046e-01	Vh
k_m	0.5	1	8.028e-01	
k_n	-0.2	0.2	5.859e-02	

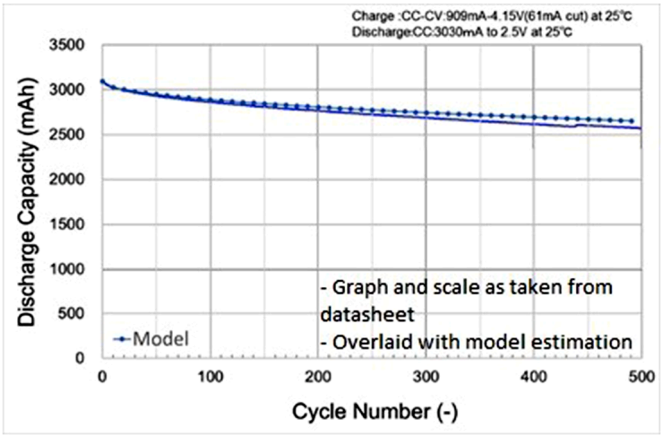

Figure 9. Model vs Datasheet Estimation.

model. This may be connected to the difference in initial capacity or a general overestimation for the purposes of performance guarantee. These biases may be taken into account during the application of DREMUS, but the overall estimation shows nearly identical behaviour and ageing rate.

Sensitivity Analysis

To perform a sensitivity analysis on the ageing model, the three key parameters are investigated: temperature, C-rate and SoC. Since all of these parameters are in the exponent of the formula, their impact will be considered on the logarithmic scale.

$$\log\left(\frac{dDeg_{lin}}{dt}\right) = Y = log(k_1) + \left(-\frac{k_2}{T}(U_n - k_3 - k_4 c)\right) \tag{36}$$

As reference conditions 50 % SoC, 20°C and 0 C are chosen. The boundary conditions are 0-100 % SoC, 0 to 40°C and +2 to -2 C and will be used for normalisation. The average values for the derivative change under these conditions are given in Table 7.

This shows clearly, how the ageing is mainly dependent on the charging and discharging current of the cell. The temperature has the least influence, which is likely due to its relatively small change on the Kelvin scale.

Hence, the charge power/current of the model will have the most significant impact on the ageing. However, since the impact of SoC and temperature are also captured, the calendric degradation will be covered as well.

Table 7
Average normalised sensitivities of the ageing model.

$\frac{dY}{dSoC}(SoC^{max} - SoC^{min})$	0.540968
$\frac{dY}{dT}(T^{max} - T^{min})$	0.0314
$\frac{dY}{dc}(c^{max} - c^{min})$	11.94867

Application to other Models

To be applicable to other cell types another factor must be introduced in the ageing equation representing the ageing speed under the conditions provided in the battery documentation.

$$Deg_{lin} = k_{ds}\int k_1 \exp\left(-\frac{k_2}{T}(U_n - k_3 - k_4 c)\right)dt \tag{37}$$

For the given cell type A, k_{ds} equals to 1. For other cells, the ageing rate must be determined using the reference conditions given in datasheet or warranty to reach EOL. Using the electrical and thermal model, the profiles for T, SoC and C-rate can be determined, and k_{ds} can be calculated as follows:

$$k_{ds} = \frac{1}{\int_{t_0}^{t_{eol}} k_1 \exp\left(-\frac{k_2}{T}(U_n - k_3 - k_4 c)\right)dt} \tag{38}$$

Since the ageing rate is determined using the same models and base assumptions, it will provide the same result as given by the manufacturer under the same conditions.

Methods of Application

Now that all three models have been assembled and individually verified, they can be used to model BESS. Since DREMUS contains a full simulation, any desired point of interest (SoH, SoC, temperature etc.) can be determined from it. This section, however, specifically outlines how it can be used to fulfil the mentioned necessary purposes.

Figure 10 describes the process for the analysis of a BESS project using DREMUS. First, using the determination of the ageing factors the performance of different systems can be compared. Then, after consideration of both performance and cost factors the best suitable BESS can be selected. The impact of the services on the system can be determined and compared the same way. In the end the overall project can be evaluated.

The process is explained in more detail in the following.

Battery Performance Comparison and Selection

This is mainly enabled by calculating k_{ds} for different BESS units. A lower k_{ds} displays a lower ageing rate and therefore a longer lifetime under identical utilisation. For instance, a storage system with a k_{ds} value of 2 would reach 80 % capacity twice as fast under identical conditions as the tested cells.

The premise for this comparison is that the end-of-life SoH for all investigated batteries is 80 %. The equations must be adjusted accordingly under other circumstances and both k_{ds} and $SoH_{abs,eol}$ must be weighed against the priorities of the application (e.g. a battery with a capacity below 80 % may be unsuitable for applications with high energy requirements). It also should be noted, that an approach with lower EOL capacity will still result in a square-root-of-time dependency with the current model.

For mission profiles with high power/energy requirements, the model can also be used to identify changes in the capabilities to provide power/energy over time. For example, the maximum discharge power would be determined by the lower voltage limit.

The performance capabilities should always be weighed against the financial and logistical factors of the storage system when selecting the ideal BESS.

BESS Service Comparison

Assuming that within a given time frame, two or more services (or combination of services) can be provided by a BESS, each of the services mission profiles can be applied to the model. Ideally, the model should

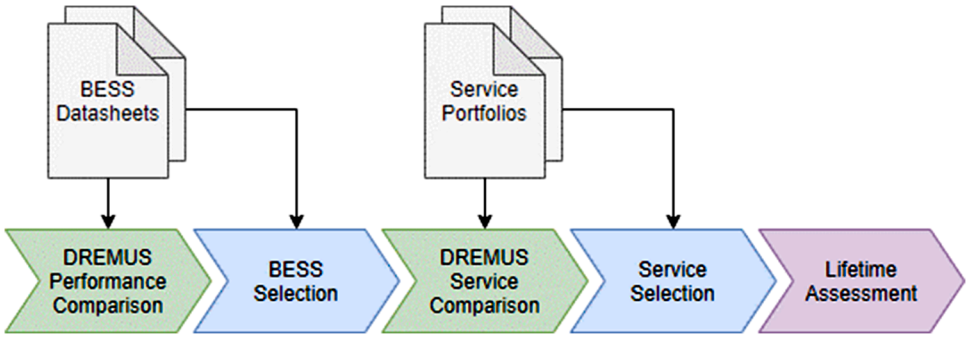

Figure 10. BESS Project Planning and Evaluation Process with DREMUS.

consider its initial SoH. The linear degradation incurred can either be compared directly, or connected to the generated value of each mission profile as follows:

$$\frac{Value}{Deg_{lin}} = Degradation\ Value \tag{39}$$

The monetary value of a provided service and the degradation incurred by it have to cover identical time periods and must include any preparation (such as recharge for ancillary services) or idle periods (for time specific services). The degradation value in £/% expresses how much monetary value the battery generated by sacrificing its lifetime.

It also provides an indication of how much value the BESS would potentially be able to generate if it were to provide that service permanently and can be compared against its purchasing costs. For instance, a service that, on average, generates 100 £ in value and reduces the battery's SoH by 0.1 % would generate an absolute value of 100.000 £ in the lifetime of the BESS.

For a thorough assessment, contractual durations as well as prospective value changes should be taken into account. For instance, arbitrage trading can be provided flexibly, but its profit is particularly sensitive to local market and energy system developments.

BESS Lifetime Assessment

Once a prediction of mission profiles and revenue streams for the BESS lifetime is available, the model can be applied for a full lifetime-model, where the BESS is simulated to provide the most profitable services until reaching its EOL condition.

The data can then be used to determine the full value and commercial return of the BESS. In contrast to the estimate provided by the degradation value, discount rates, market-development and any additionally incurred cashflow (e.g. operation, maintenance) should be considered to accurately determine its internal rate of return and net present value.

Evaluation and Discussion

The modelling approach presented allows for a multi-physics assessment of BESS without the need for detailed or historical data on the battery. Every parameter outlined is relative, making the model applicable to any scale of BESS and, due to the linearization of the ageing behaviour, both battery long term performance and the value and damage of mission profiles can be directly assessed and compared. Due to the model's structure it can also be enhanced by additionally available data to increase its precision for existing BESS.

By tackling the issues mentioned in the introduction, this model will contribute to the third-party purchasers assessment of BESS and now allow for a realistic judgement of market-viable options. This increase in tangibility of business cases may act to promote BESS as independent value generating assets on one hand and as long-term grid supporting elements on the other hand. It further allows for a more efficient use of BESS, especially in the context of support for renewable energy sources and grid sustainability.

However, several aspects need to be taken into account when using this approach. Firstly, due to the requirements and premises of the model, several restrictions apply to it. The model should not be used on the BESS if:

- The cell temperature is expected to fall below 10 or rise above 40°C.
- The cell chemistry is not graphite-based Li-Ion.
- The battery is subject to other environmental stresses (e.g. vibration).

Secondly, all parameters and models are provided to work with the minimum required data to form a full multi-physics estimation of a generic BESS. If more detailed data or models are available for the specific use case, they should be used instead.

Thirdly, while the sub-models have been individually verified, a full system verification is desired. This verification requires system level degradation data, which takes longer time to generate and is outside the scope of this article. We aim to discuss the performance and verification of DREMUS model in a future article when these data will be available.

The precision of the model is limited by the precision of the data the manufacturer provides. It should be kept in mind that DREMUS is not designed to provide precise ageing behaviour, but rather best possible approximation based on available data to third parties.

Data Availability

The measurement data collected in this project is available from the corresponding author on request. Restrictions apply for data of commercial cells.

DREMUS Parameters

Constants	
R_g	Boltzmann Constant
Parameter	
η	Efficiency
κ	Conductivity
τ	Time Constant
c	C-rate
C	Capacitance
Deg	Degradation
E	Energy
I	Current
k	Fitting parameter
m	Cell series count
n	Cell string count
P	Power
q	Heat
Q	Coulombic Capacity
R	Resistance

(*continued on next page*)

(*continued*)

SoC	State of Charge
SoH	State of Health
t	Time
T	Temperature
U	Voltage
Sub- and Superscripts	
a	Activation
abs	Absolute
amb	Ambient
bat	Battery
cell	Cell
ch	Charge
con	Converter
conv	Convection
DC	Direct current
ds	Datasheet
dch	discharge
ent	Entropy
eol	End-of-life
in	Input
lin	Linear
max	Maximal
min	Minimal
mod	Module
n	Nominal
oc	Open-circuit
ohm	Ohmic
out	Output
r	Roundtrip
reac	Reaction
ref	Reference
res	Resistive
side	Side
u	Unidirectional
%	Percent (relative value)

Author Statement

We would like to submit the revised review article entitled "DREMUS: A Data-Restricted Multi-Physics Simulation Model for Lithium-Ion Battery Storage" for consideration for publication in the *Journal of Energy Storage*.

We have now addressed all of reviewers' questions, comments and suggestions. The subsequent improvements are clearly listed in a separate document titled 'Response to Reviewer' and highlighted in red within the manuscript to further facilitate the review process.

We hope that the improved paper is clearer and better present the review. The authors would like to take this opportunity to again thank the reviewers for their efforts in reviewing our manuscript and their insightful comments.

The guidelines for submission were adhered to and as per the guidance for publication, figures are provided. We sincerely hope that our updated manuscript is now suitable for publication in your esteemed journal.

Declaration of Competing Interest

The authors declare that they have no known competing financial interests or personal relationships that could have appeared to influence the work reported in this paper.

Acknowledgement

This project has been made possible through the EPSRC Centre for Doctoral Training in Sustainable Materials and Manufacturing (grant number: EP/L016389/1) and funding from EDF Energy. Additional research also presented in the paper was undertaken in collaboration with the WMG Centre High Value Manufacturing Catapult (funded by Innovate UK) in collaboration with Jaguar Land Rover.

Supplementary materials

Supplementary material associated with this article can be found, in the online version, at doi:10.1016/j.est.2020.102051.

Bibliography

[1] L. Huat, Y. Ye, A.A.O. Tay, Integration issues of lithium-ion battery into electric vehicles battery pack, J. Clean. Prod. 113 (2016) 1032–1045. https://doi.org/10.1016/j.jclepro.2015.11.011.

[2] C.R. Birkl, M.R. Roberts, E. Mcturk, P.G. Bruce, D.A. Howey, Degradation diagnostics for lithium ion cells, J. Power Sources. 341 (2016) 373–386. https://doi.org/10.1016/j.jpowsour.2016.12.011.

[3] A. Barai, K. Uddin, M. Dubarry, L. Somerville, A. McGordon, P. Jennings, I. Bloom, A comparison of methodologies for the non-invasive characterisation of commercial Li-ion cells, Prog. Energy Combust. Sci. 72 (2019) 1–31. https://doi.org/10.1016/j.pecs.2019.01.001.

[4] B. Foggo, N. Yu, Improved battery storage valuation through degradation reduction, IEEE Trans. Smart Grid. 9 (2018) 5721–5732. https://doi.org/10.1109/TSG.2017.2695196.

[5] K. Uddin, R. Gough, J. Radcliffe, J. Marco, P. Jennings, Techno-economic analysis of the viability of residential photovoltaic systems using lithium-ion batteries for energy storage in the United Kingdom, Appl. Energy. 206 (2017) 12–21. https://doi.org/10.1016/j.apenergy.2017.08.170.

[6] A. Perez, R. Moreno, R. Moreira, M. Orchard, G. Strbac, Effect of Battery Degradation on Multi-Service Portfolios of Energy Storage, IEEE Trans. Sustain. Energy. 7 (2016) 1718–1729. https://doi.org/10.1109/TSTE.2016.2589943.

[7] X. Jian, L. Zhang, Unit commitment considering reserve provision by wind generation and storage, in: Asia-Pacific Power Energy Eng. Conf. APPEEC. 2016-Decem, 2016, pp. 8–12. https://doi.org/10.1109/APPEEC.2016.7779460.

[8] K. Abdulla, J. De Hoog, V. Muenzel, F. Suits, K. Steer, A. Wirth, S. Halgamuge, Optimal Operation of Energy Storage Systems Considering Forecasts and Battery Degradation, IEEE Trans. Smart Grid. PP (2016) 1–11. https://doi.org/10.1109/TSG.2016.2606490.

[9] A. Mamun, I. Narayanan, D. Wang, A. Sivasubramaniam, H.K. Fathy, Multi-objective optimization of demand response in a datacenter with lithium-ion battery storage, J. Energy Storage. 7 (2016) 258–269. https://doi.org/10.1016/j.est.2016.08.002.

[10] D. Pelzer, D. Ciechanowicz, A. Knoll, A.K.D. Pelzer, D. Ciechanowicz, Energy arbitrage through smart scheduling of battery energy storage considering battery degradation and electricity price forecasts, IEEE PES Innov. Smart Grid Technol. Conf. Eur. (2016) 472–477. https://doi.org/10.1109/ISGT-Asia.2016.7796431.

[11] National Renewable Energy Laboratory (NREL), J. Neubauer, Battery Lifetime Analysis and Simulation Tool (BLAST) Documentation, 2014. https://doi.org/NREL/TP-5400-63246.

[12] F. Wankmüller, P.R. Thimmapuram, K.G. Gallagher, A. Botterud, Impact of battery degradation on energy arbitrage revenue of grid-level energy storage, J. Energy Storage. 10 (2017) 56–66. https://doi.org/10.1016/j.est.2016.12.004.

[13] M. Swierczynski, D.I. Stroe, A.I. Stan, R. Teodorescu, D.U. Sauer, Selection and performance-degradation modeling of limo2/li 4ti5o12 and lifepo4/c battery cells as suitable energy storage systems for grid integration with wind power plants: An example for the primary frequency regulation service, IEEE Trans. Sustain. Energy. 5 (2014) 90–101. https://doi.org/10.1109/TSTE.2013.2273989.

[14] B. Lian, A. Sims, D. Yu, C. Wang, R.W. Dunn, Optimizing LiFePO4 Battery Energy Storage Systems for Frequency Response in the UK System, IEEE Trans. Sustain. Energy. 8 (2017) 385–394. https://doi.org/10.1109/TSTE.2016.2600274.

[15] D.I. Stroe, M. Swierczynski, A.I. Stroe, R. Laerke, P.C. Kjaer, R. Teodorescu, Degradation Behavior of Lithium-Ion Batteries Based on Lifetime Models and Field Measured Frequency Regulation Mission Profile, IEEE Trans. Ind. Appl. 52 (2016) 5009–5018. https://doi.org/10.1109/TIA.2016.2597120.

[16] C. Zhang, J. Jiang, L. Zhang, S. Liu, L. Wang, P.C. Loh, A generalized SOC-OCV model for lithium-ion batteries and the SOC estimation for LNMCO battery, Energies 9 (2016). https://doi.org/10.3390/en9110900.

[17] R.E. Williford, V.V. Viswanathan, J.G. Zhang, Effects of entropy changes in anodes and cathodes on the thermal behavior of lithium ion batteries, J. Power Sources. 189 (2009) 101–107. https://doi.org/10.1016/j.jpowsour.2008.10.078.

[18] P. Keil, A. Jossen, Aging of Lithium-Ion Batteries in Electric Vehicles : Impact of Regenerative Braking, 7 (2015) 41–51.

[19] C. Betzin, H. Wolfschmidt, M. Luther, Electrical operation behavior and energy efficiency of battery systems in a virtual storage power plant for primary control reserve, Int. J. Electr. Power Energy Syst. 97 (2018) 138–145. https://doi.org/10.1016/j.ijepes.2017.10.038.

[20] A. Cordoba-arenas, S. Onori, G. Rizzoni, A control-oriented lithium-ion battery pack model for plug-in hybrid electric vehicle cycle-life studies and system design with consideration of health management, J. Power Sources. 279 (2015) 791–808. https://doi.org/10.1016/j.jpowsour.2014.12.048.

[21] K. Smith, A. Saxon, M. Keyser, B. Lundstrom, Z. Cao, A. Roc, Life Prediction Model for Grid - Connected Li - ion Battery Energy Storage System, (2017) 4062–4068.

[22] Z. He, D. Guo, X. Liu, G. Yang, An Evaluation Method of Battery DC Resistance Consistency Caused by Temperature Variation, in: IEEE 2017 20th Int. Conf. Electr. Mach. Syst., 2017. https://doi.org/10.1109/ICEMS.2017.8056426.

[23] M. Shadman Rad, D.L. Danilov, M. Baghalha, M. Kazemeini, P.H.L. Notten, Adaptive thermal modeling of Li-ion batteries, Electrochim. Acta. 102 (2013) 183–195. https://doi.org/10.1016/j.electacta.2013.03.167.

[24] L. Zheng, J. Zhu, G. Wang, D.D.C. Lu, P. McLean, T. He, Experimental analysis and modeling of temperature dependence of lithium-ion battery direct current resistance for power capability prediction, in: 2017 20th Int. Conf. Electr. Mach. Syst. ICEMS 2017, 2017, pp. 0–3. https://doi.org/10.1109/ICEMS.2017.8056426.
[25] X. Gong, Modeling of Lithium-ion Battery Considering Temperature and Aging Uncertainties, 2016. https://deepblue.lib.umich.edu/bitstream/handle/2027.42/134041/GongDissertationFinal.pdf?sequence=1&isAllowed=y (accessed August 24, 2018).
[26] S. Käbitz, J.B. Gerschler, M. Ecker, Y. Yurdagel, B. Emmermacher, D. André, T. Mitsch, D.U. Sauer, Cycle and calendar life study of a graphite|LiNi1/3Mn 1/3Co1/3O2 Li-ion high energy system. Part A: Full cell characterization, J. Power Sources. 239 (2013) 572–583. https://doi.org/10.1016/j.jpowsour.2013.03.045.
[27] R.B. Wright, C.G. Motloch, J.R. Belt, J.P. Christophersen, C.D. Ho, R.A. Richardson, I. Bloom, S.A. Jones, V.S. Battaglia, G.L. Henriksen, T. Unkelhaeuser, D. Ingersoll, H.L. Case, S.A. Rogers, R.A. Sutula, Calendar- and cycle-life studies of advanced technology development program generation 1 lithium-ion batteries, J. Power Sources. 110 (2002) 445–470. https://doi.org/10.1016/S0378-7753(02)00210-0.
[28] A. Suttman, Lithium Ion Battery Aging Experiments and Algorithm Development for Life Estimation, (2011) 1–105. http://rave.ohiolink.edu/etdc/view?acc_num=osu1306937891.
[29] A. Nikolian, J. Jaguemont, J. de Hoog, S. Goutam, N. Omar, P. Van Den Bossche, J. Van Mierlo, Complete cell-level lithium-ion electrical ECM model for different chemistries (NMC, LFP, LTO) and temperatures (−5°C to 45°C) – Optimized modelling techniques, Int. J. Electr. Power Energy Syst. 98 (2018) 133–146. https://doi.org/10.1016/j.ijepes.2017.11.031.
[30] H. He, R. Xiong, J. Fan, Evaluation of lithium-ion battery equivalent circuit models for state of charge estimation by an experimental approach, Energies 4 (2011) 582–598. https://doi.org/10.3390/en4040582.
[31] A. Rahmoun, H. Biechl, Modelling of Li-ion batteries using equivalent circuit diagrams, Prz. Elektrotechniczny. 88 (2012) 152–156. http://red.pe.org.pl/articles/2012/7b/40.pdf.
[32] S. Abu-sharkh, D. Doerffel, Rapid test and non-linear model characterisation of solid-state lithium-ion batteries, 130 (2004) 266–274. https://doi.org/10.1016/j.jpowsour.2003.12.001.
[33] L. Pei, T. Wang, R. Lu, C. Zhu, Development of a voltage relaxation model for rapid open-circuit voltage prediction in lithium-ion batteries, J. Power Sources. 253 (2014) 412–418. https://doi.org/10.1016/j.jpowsour.2013.12.083.
[34] A.W. Golubkov, S. Scheikl, R. Planteu, G. Voitic, H. Wiltsche, C. Stangl, G. Fauler, A. Thaler, V. Hacker, Thermal runaway of commercial 18650 Li-ion batteries with LFP and NCA cathodes - Impact of state of charge and overcharge, RSC Adv 5 (2015) 57171–57186. https://doi.org/10.1039/c5ra05897j.
[35] Y. Hua, M. Xu, M. Li, C. Ma, C. Zhao, Estimation of state of charge for two types of lithium-ion batteries by nonlinear predictive filter for electric vehicles, Energies 8 (2015) 3556–3577. https://doi.org/10.3390/en8053556.
[36] U. Iraola, I. Aizpuru, J.M. Canales, A. Etxeberria, I. Gil, Methodology for thermal modelling of lithium-ion batteries, IECON Proc. (Industrial Electron. Conf. (2013) 6752–6757. https://doi.org/10.1109/IECON.2013.6700250.
[37] R. Srinivasan, A.C. Baisden, B.G. Carkhuff, M.H. Butler, A. Carson Baisden, B. G. Carkhuff, M.H. Butler, The five modes of heat generation in a Li-ion cell under discharge, J. Power Sources. 262 (2014) 93–103. https://doi.org/10.1016/j.jpowsour.2014.03.062.
[38] Y. Reynier, R. Yazami, B. Fultz, The entropy and enthalpy of lithium intercalation into graphite, J. Power Sources. 119–121 (2003) 850–855. https://doi.org/10.1016/S0378-7753(03)00285-4.
[39] D. Bernardi, A General Energy Balance for Battery Systems, J. Electrochem. Soc. 132 (1985) 5. https://doi.org/10.1149/1.2113792.
[40] J. Newman, K.E. Thomas, H. Hafezi, D.R. Wheeler, Modeling of lithium-ion batteries, J. Power Sources. 119–121 (2003) 838–843. https://doi.org/10.1016/S0378-7753(03)00282-9.
[41] T.R. Tanim, C.D. Rahn, Aging formula for lithium ion batteries with solid electrolyte interphase layer growth, J. Power Sources. 294 (2015) 239–247. https://doi.org/10.1016/j.jpowsour.2015.06.014.
[42] R. Spotnitz, Simulation of capacity fade in lithium-ion batteries, J. Power Sources. 113 (2003) 72–80. https://doi.org/10.1016/S0378-7753(02)00490-1.
[43] M. Safari, M. Morcrette, A. Teyssot, C. Delacourt, Multimodal physics-based aging model for life prediction of Li-Ion batteries, J. Electrochem. Soc. (2009) 156. https://doi.org/10.1149/1.3043429.
[44] P. Ramadass, B. Haran, P.M. Gomadam, R. White, B.N. Popov, Development of First Principles Capacity Fade Model for Li-Ion Cells, J. Electrochem. Soc. 151 (2004) 196–203. https://doi.org/10.1149/1.1634273.
[45] M. Broussely, S. Herreyre, P. Biensan, P. Kasztejna, K. Nechev, R.J. Staniewicz, Aging mechanism in Li ion cells and calendar life predictions, J. Power Sources. 97–98 (2001) 13–21. https://doi.org/10.1016/S0378-7753(01)00722-4.
[46] I. Bloom, B.W. Cole, J.J. Sohn, S.A. Jones, E.G. Polzin, V.S. Battaglia, G. L. Henriksen, C. Motloch, R. Richardson, T. Unkelhaeuser, D. Ingersoll, H.L. Case, An accelerated calendar and cycle life study of Li-ion cells, J. Power Sources. 101 (2001) 238–247. https://doi.org/10.1016/S0378-7753(01)00783-2.
[47] C. Julien, A. Mauger, A. Vijh, K. Zaghib, Lithium Batteries - Science and Technology, 1995. https://doi.org/10.1007/978-3-319-19108-9.
[48] E. Sarasketa-Zabala, E. Martinez-Laserna, M. Berecibar, I. Gandiaga, L. M. Rodriguez-Martinez, I. Villarreal, Realistic lifetime prediction approach for Li-ion batteries, Appl. Energy. 162 (2016) 839–852. https://doi.org/10.1016/j.apenergy.2015.10.115.
[49] M. Ecker, J.B.B. Gerschler, J. Vogel, S. Käbitz, F. Hust, P. Dechent, D.U.U. Sauer, Analyzing calendar aging data towards a lifetime prediction model for lithium-ion batteries, 26th Electr, Veh. Symp. 2012 (1) (2012) 47–58.
[50] T. Waldmann, M. Wilka, M. Kasper, M. Fleischhammer, M. Wohlfahrt-Mehrens, Temperature dependent ageing mechanisms in Lithium-ion batteries - A Post-Mortem study, J. Power Sources. 262 (2014) 129–135. https://doi.org/10.1016/j.jpowsour.2014.03.112.
[51] K. Uddin, S. Perera, W.D. Widanage, L. Somerville, J. Marco, Characterising lithium-ion battery degradation through the identification and tracking of electrochemical battery model parameters, Batteries 2 (2016) 13. https://doi.org/10.3390/batteries2020013.
[52] N. Legrand, B. Knosp, P. Desprez, F. Lapicque, Physical characterization of the charging process of a Li-ion battery and prediction of Li plating by electrochemical modelling, J. Power Sources. 245 (2014) 208–216. https://doi.org/10.1016/j.jpowsour.2013.06.130.
[53] M. Kassem, J. Bernard, R. Revel, S. Pélissier, F. Duclaud, C. Delacourt, Calendar aging of a graphite/LiFePO 4 cell, J. Power Sources. 208 (2012) 296–305. https://doi.org/10.1016/j.jpowsour.2012.02.068.